Influence of gas adsorption induced non-uniform deformation on the evolution of coal permeability

Mingyao Wei[a,*], Jishan Liu[b], Derek Elsworth[c], Shaojun Li[a], Fubao Zhou[d,e]

[a] State Key Laboratory of Geomechanics and Geotechnical Engineering, Institute of Rock and Soil Mechanics, Chinese Academy of Sciences, Wuhan 430071, China
[b] Department of Chemical Engineering, School of Engineering, The University of Western Australia, ø35 Stirling Highway, Perth, WA 6009, Australia
[c] Department of Energy and Mineral Engineering, G3 Center and Energy Institute, The Pennsylvania State University, University Park, PA 16802, USA
[d] Faculty of Safety Engineering, China University of Mining & Technology, Xuzhou, Jiangsu 221116, China
[e] Key Laboratory of Gas and Fire Control for Coal Mines (Ministry of Education), China University of Mining & Technology, Xuzhou, Jiangsu 221116, China

ABSTRACT

When adsorbing gas is injected into coal, the gas fills in the fractures quickly and a pressure difference between matrix and fractures is created. Because of this difference, there is a pressure gradient within the matrix. The gradient evolves with time from the initial equilibrium (zero gradient) to the final equilibrium (zero gradient), so does the adsorption–swelling induced matrix deformation. Previous studies have not taken this effect into consideration. In this study, we hypothesize that the pressure gradient affects the expansion of the gas-invaded area/volume with the matrix and the propagation of the expansion front creates a non-uniform deformation within the matrix. Under this hypothesis, a relation between coal permeability and the expansion of the gas-invaded area with the matrix can be established. When the gas-invaded area is localized in the vicinity of the fracture wall, the expansion of the matrix within this area narrows the fracture opening. We define this as local swelling/shrinking. This local swelling/shrinking is controlled primarily by the coal internal structure. When the gas-invaded area is further spread over the matrix, the expansion of the whole matrix may narrow or widen the fracture opening depending on the external boundary conditions. This global swelling/shrinking is controlled primarily by the external boundary conditions. These conceptual understandings are defined through strain rate-based coal permeability models for both the matrix and the fractures. This strain rate based time-dependent permeability model was verified against experimental observations, that couples coal deformation, the gas flow in the matrix system and gas flow in the fracture system.

1. Introduction

Coal permeability in coal seam is a key controlling factor for the coalbed methane (CBM) extraction. It has been widely studied through both laboratory measurements and modelling over past few decades. Previous experimental studies have shown that the coal permeability mainly depends on the coal fractures under the influences of external stresses and gas pressure.[1–9] When the gas pressure decreases, the fracture will be mechanically close due to the rising effective stress. This leads to the decrease of coal permeability. While the matrix shrinkages after gas desorption out of coal, and thus increase coal permeability. A number of coal permeability models have been developed to account for the mechanisms mentioned above.[10–12]

The dual porosity and dual permeability models were widely applied to characterize coal reservoir. The interactions between coal matrix and fractures are normally defined by the gas mass exchange term. The mechanical interaction between fractures and coal matrix during coal deformation is not considered in all the permeability models. Since the mechanical properties between coal matrix and fracture are dramatically different, the interaction can cause a significant effect on permeability changes under certain conditions[13] where it is difficult to predict the evolution of permeability. These problematic behaviors have attracted growing attention from researchers.[14–17] Compared with the flow in conventional reservoirs, gas flow in an unconventional reservoir is subject to more nonlinear, coupled processes. Liu et al.[18] elucidated the role of the transition of coal matrix swelling, from local swelling to macro-swelling, under high differential pressure on the evolution of permeability. This highlights the role of mechanical interaction between matrix and fracture. Because of the high contrast of permeability between fractures and matrix, the diffusion process from fracture to matrix lasts for an extended period, potentially from a few months to years following the initiation of gas

injection. As gas propagates from the fracture wall into the matrix, the gas-invaded volume expands through the matrix, creating a non-uniform swelling zone. A few results of experimental tests have documented the importance of the interaction of mechanical deformation.[19–25] Liu et al.[18] conducted an explicit simulation to verify dynamic interactions between coal matrix swelling/shrinkage and fracture aperture alteration, and translations of these interactions to permeability evolution under unconstrained swellings. The model predictions are consistent with typical laboratory and in-situ observations documented within the literature. Peng et al.[15] proposed a continuous permeability model that characterizes the matrix-fracture interactions. The effective strain affected fracture permeability is divided into global strain and local strain subjectively. The results imply that the coal permeability profiles regulated primarily by the matrix diffusivity. The "V" shape profile represents that the transition of coal permeability from the initial equilibrium state to final equilibrium state takes a long period of time. In another word, the strain in matrix takes long period of time to reach final equilibrium when matrix diffusivity is low. However, the assumption is inconsistent with real physical processes. Zhang et al.[26] investigated the deformation compatibility between the matrix and the fracture. It provide compelling evidence that coal permeability is closely related to the expansion of gas invaded volume from fracture into matrix. The transition from local (to the fracture) swelling to global depends on the distribution of matrix strain. Based on these previous understandings, the resultant matrix strain of gas invasion controls permeability evolution.

It has been demonstrated that the interaction between matrix and fracture controls the evolution of coal permeability. However, there is currently no suitable continuous model that includes this mechanism. In this paper, this important mechanism was incorporated. We hypothesize that the gas diffusion-induced non-uniform deformation in coal matrix has been responsible for this interaction under the conditions of constant confining stresses. In the following sections, we first apply the conventional poroelasticity theory to simulate the exact responses to coal permeability to gas injection under the constant confining stresses. We formulate a strain rate based permeability model that couples coal deformation and gas flows in both fractures and matrix as a set of partial differential equations. These equations are then solved using a commercial tool.

2. Conceptual validation of the hypothesis

The goal of this section is to conceptually prove our hypothesis through a simple model. We consider a controlled volume in which a fracture is embedded in the coal matrix, as illustrated in Fig. 1. Gas is injected through the fracture. When gas is injected, it fills up the
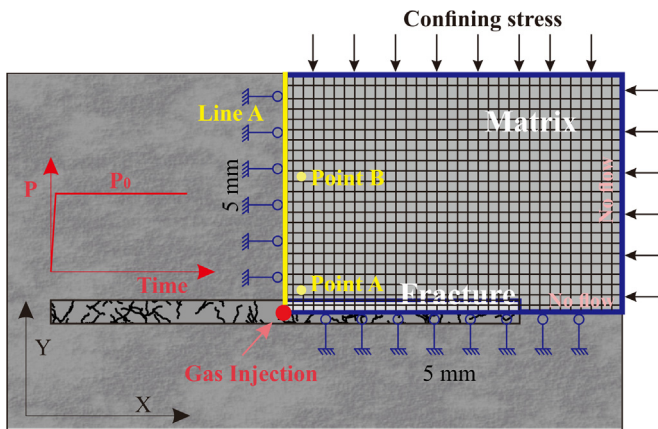

Fig. 1. A model of gas injection into coal with an embedded fracture under constant confining stresses. Due to symmetry, a quarter of the model was selected for the simulation.

fracture instantly. Therefore, the gas pressure in the fracture reaches the injection pressure. The gas pressure changes from zero (before the injection) to the injection pressure (after the injection) inflates the fracture from the initial opening to a new magnitude. It results in the increase of fracture permeability. If the injection pressure maintains as a constant, gas diffuses from the fracture into the matrix. This diffusion-induced the interaction between the matrix and the fracture affects the evolution of the fracture opening.

2.1. Modelling approach

Due to the symmetry, a quarter of the controlled volume is selected. The model length is 5 mm while the height is also 5 mm. The length of fracture is 3 mm and the aperture is 0.1 mm. The fracture structure is modeled explicitly which is embedded in the matrix. A constant confining stress is applied on the top and right boundaries. It is assumed that absorbing gas is injected at the left-bottom corner of the model. No flow conditions are applied on all boundaries. The mass exchange between the matrix and fracture occurs on the connection boundary. The geometry boundary condition between matrix domain and fracture domain is pressure continuity across interior boundary. We assume that the matrix is homogeneous and elastic, and its deformation obeys the Hooke's law. The fracture is also assumed as homogeneous and elastic with much lower Young's modulus. According to the theory of continuum mechanics, the deformation of the homogeneous, isotropic, and uniform elastic medium can be described by the Navier-type equation[27]:

$$Gu_{i,kk} + \frac{G}{1-2v}u_{k,ik} - \alpha p - K\varepsilon_L \frac{L_b}{(p+L_b)^2}p_i + f_i = 0 \tag{1}$$

where G the shear modulus, u_i is the component of displacement in the i-direction, ν the Possion's ratio, α is the Biot coefficient, K is the bulk modulus, ε_L is the Langmuir volumetric strain constant representing the volumetric strain at infinite pore pressure. L_b is the Langmuir pressure at which the measured volumetric strain is equal to $0.5\varepsilon_L$, p is the pore pressure, f_i is the component of body force in the i –direction.

The flow in both fracture and matrix is assumed to be governed by Darcy's law. For the case of an ideal absorbing gas, the governing equations for matrix and fracture are:

$$\frac{d}{dt}\left(\phi_m p_m \frac{M}{RT} + (1-\phi_m)\rho_s\rho_a \frac{L_a p_m}{p_m + L_b}\right) - \nabla\left(\rho_g \frac{k_m}{\mu}\nabla p_m\right) = 0 \tag{2}$$

$$\frac{d}{dt}\left(\phi_f p_f \frac{M}{RT}\right) - \nabla\left(\rho_g \frac{k_f}{\mu}\nabla p_f\right) = 0 \tag{3}$$

where ϕ_m and ϕ_f are the porosity of matrix and fracture system, respectively, p_m and p_f are the gas pressure in matrix and fracture systems, M is the molecular mass of gas, R is the universal gas constant, T is the absolute gas temperature, ρ_s is coal density, ρ_a is gas density at atmospheric pressure, L_a is the Langmuir volume constant, ρ_g is the gas density, k_m and k_f are the permeability of matrix and fracture system. All the parameters for fracture and matrix system in simulation model are listed in Table 1. The resulting governing equations are a set of nonlinear partial differential equations (PDEs) that are second order in space and first order in time. These equations are implemented and solved numerically using COMSOL Multiphysics.

2.2. Modelling results

For the purpose of comparison, we modeled two cases with different ratios of the fracture permeability to the matrix permeability. We set these ratios as 1 and 100 respectively. In the following analysis, we look at the evolutions of the effective strain in the matrix along the Line A, and at Point A and Point B as shown in Fig. 1. The modelling results are shown in Figs. 2 through 5. Evolutions of the effective strain in the coal

Table 1
Property parameters of explicit model.

Parameters	Value
Young's modulus of matrix	10 GPa
Young's modulus of fracture	2 GPa
Langmuir volume	0.0017 m^3/kg
Langmuir pressure	1.2 MPa
Langmuir volumetric strain	0.002
Possion's ratio of matrix	0.27
Possion's ratio of fracture	0.27
Porosity of matrix	0.02
Porosity of fracture	0.02
Permeability of matrix	1×10^{-19} m^2
Permeability of fracture	1×10^{-17} m^2
Fracture aperture	0.1 mm
Injection pressure, P_0	6 MPa
Confining stress	26 MPa

matrix are shown in Fig. 2. The positive sign denotes the swelling (extensive) strain while the negative sign denotes the shrinking (compressive) strain. When the permeability ratio is equal to 1, it represents the single porous medium. The swelling strain along Line A evolves from the initial value (zero) to the maximum when the pore pressure reaches the injection pressure everywhere. Although the swelling strain increases as the gas propagates from the injection point into the matrix, the strain is almost uniform along the Line A.

When the permeability ratio is equal to 100, the effective strain changes dramatically along the line as well as over time. The effective strain at Point A reaches the maximum shrinking (compressive) magnitude right after the gas injection. After the injection, gas prorogates from the fracture into the matrix through diffusion. When the gas-invaded area is localized in the vicinity of the fracture wall, the effective stress in this area decreases and the localized shrinking (compressive) strain rebounds significantly. When the gas-invaded volume spreads further through the matrix, the entire matrix swells. When the entire matrix swells, the effective strain in the vicinity of the fracture switches from initial shrinking (compressive) to final swelling (extensive). The effective strain map for Line A shows both the spatial evolution of the effective matrix strain along the distance from the fracture wall to the exterior boundary and the temporal evolution from the initial injection state to final equilibrium state. For the spatial evolutions, complex
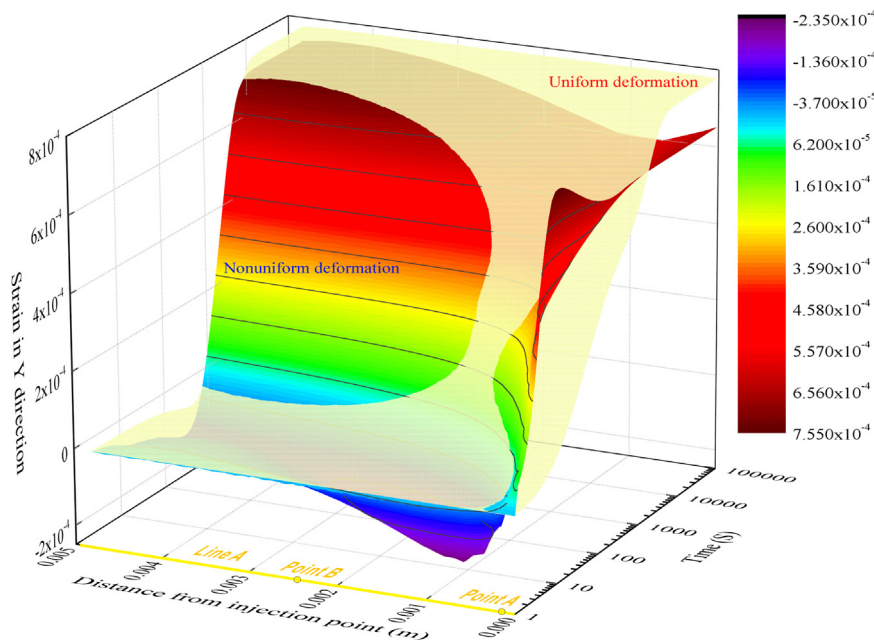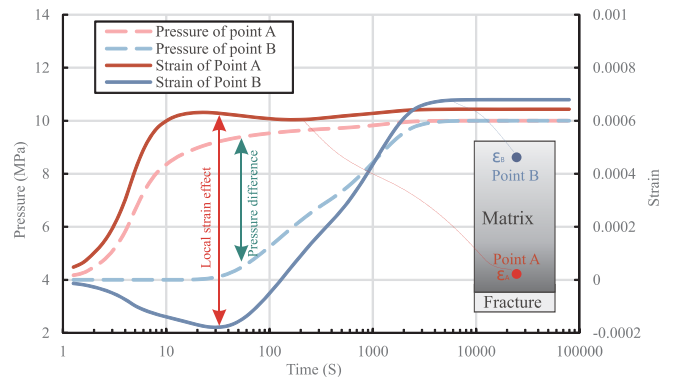

Fig. 3. Correlation between gas pressure and strain evolution.
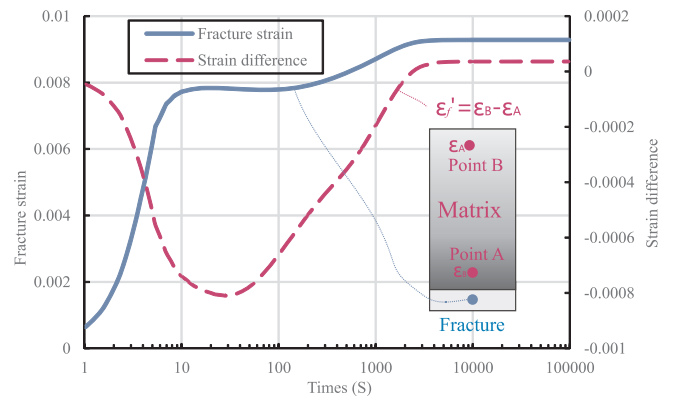

Fig. 4. The relationship between fracture strain and strain difference in matrix.

evolutions from shrinking (compressive) strain to swelling (extensive) strain can be seen in the vicinity of the fracture wall. However, only swelling (extensive) strain can be seen in the outside area.

Fig. 3 shows the correlation between strain evolution and pressure evolution at Point A and Point B. Point A is located in the vicinity of the fracture wall. Point B is located in the center of the matrix. The line linked two points is perpendicular to the fracture plane. The gas
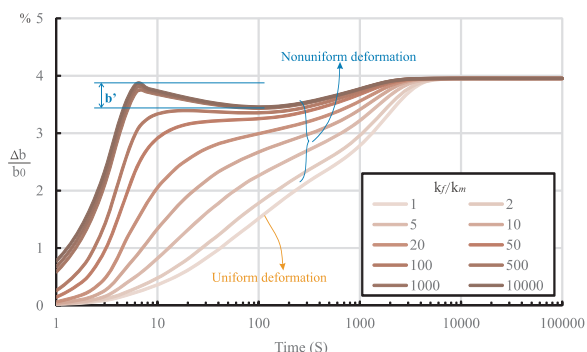

Fig. 2. Effective strain maps for two cases. (1) $k_f/k_m = 1$ (Single porous medium); (2) $k_f/k_m = 100$ (Dual porous medium).

Fig. 5. Impact of fracture to matrix permeability ratios on the evolution of the fracture aperture.

Fig. 6. Influence of local strain on conventional reservoir and unconventional reservoir.

pressure increases firstly in Point A (pink dotted line) after gas injection. Then the gas pressure in Point B (blue dotted line) begins to increase with a delay of few seconds. There always exists a gas pressure difference between these two monitor points. The gas pressure of these two points continually increase till they reach the final equilibrium state. Because of the changes in effective stress, matrix strain changes at the same time. The strain of Point A (red solid line) increase with decreasing effective stress monotonically. However, the strain of Point B (blue solid line) decreases subjected to restraint from swell deformation of Point A. When gas pressure transfers to Point B, the strain of Point B begins to increase instead of decreasing. Meanwhile, the strain of Point A in turn reduces slightly under the influence of restraint from neighboring zone. Because the Point A is located in the vicinity of the fracture wall, the fracture opening is narrowed as well. As time progresses, the final equilibrium state reaches when gas pressure equals in the entire system with the strain difference between two points vanishing in the equilibrium state.

The relationship between the fracture strain and the strain difference in matrix is shown in Fig. 4. Because of the extremely low permeability of coal matrix, the distribution of effective stress evolves with time. This evolution leads to a strain difference between Point A and Point B in the matrix. The strain difference (purple dotted line) is defined as the difference between strain of Point A and Point B. It exhibits a valley shape. A maximum magnitude of the strain difference is created immediately after the gas injection. It decreases steadily to a minimum value (the bottom of the valley), then recovers to the final steady state. It is obviously that the fracture strain is restrained when the strain difference is high enough. Furthermore, this affection vanishes when strain difference disappearances. It is evidence to indicate the corresponding relation between fracture strain and strain distribution in matrix.

Fig. 5 shows the influence of fracture-to-matrix permeability ratios on the evolution of the fracture aperture. The parameter b_0 is the initial fracture aperture with Δb representing the change in fracture aperture. In all cases, the fracture permeability remains unchanged, but the matrix permeability is different for each case. It can be seen that the aperture change is affected significantly by the permeability ratio. When the permeability ratio is equal to 1, the aperture change ratio increases from the initial state to the final equilibrium state monotonically. As the permeability ratio increases from 1 to 10,000, the curve changes from monotonical mode to bi-modular mode. When a bi-modular mode takes shape, the aperture change ratio (permeability change ratio) experiences four distinct stages: (1) increase stage; (2) decrease stage; (3) recovery stage; and (4) stable stage. The bi-modular effect becomes more significant as the fracture-to-matrix permeability ratio increases. When the matrix is highly permeable (the permeability contrast between fracture and matrix becomes less important), the bi-modular effect also diminishes. In order to compare the severity of reversal, the reduction from curve peak to valley (b′) is measured. It represents the degree of bi-modular effect on the change of
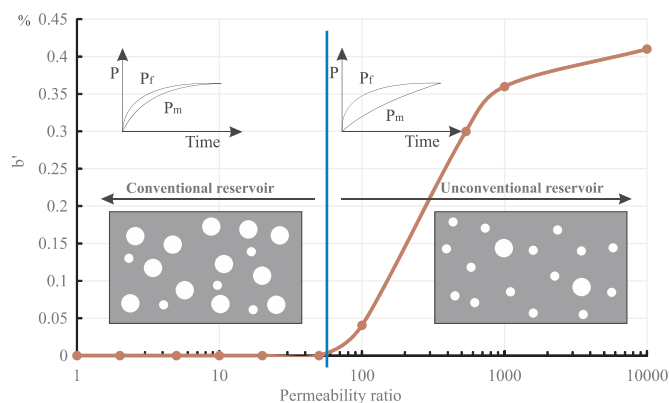
permeability. As shown in Fig. 6, the effect of non-uniform deformation on fracture permeability would be negligible because the matrix is highly permeable in the conventional reservoir. In contrast, this effect on fracture permeability is significant in the unconventional reservoir where the permeability contrast is huge. The simulation results clearly shows that the bi-modular effect is obvious for unconventional reservoir. The different between matrix and fracture is controlling factor for gas transfer between fracture and matrix. Although the matrix deformation is related to mechanical property, the differential deformation between fracture and matrix determines the bi-modular effect.

2.3. Validation of the hypothesis

Through comparing Fig. 4 and Fig. 5, a corresponding relation between the fracture aperture change ratio (fracture permeability change ratio) and the matrix strain change can be observed: (1) The permeability increase stage is corresponding to the matrix strain difference jump; (2) The permeability decrease stage is corresponding to the matrix strain decrease stage; (3) The permeability recovery stage is corresponding to the strain recovery stage; (4) The permeability stable stage is corresponding to the strain difference stable stage. These theoretical results prove our conceptual understanding. When gas is injected into shale or coal, the gas inflates the fracture almost instantly. This inflation creates the maximum strain difference in the matrix. After the injection, the gas diffuses from the fracture into the matrix. When the diffusion is localized in the vicinity of the fracture wall, the swelling of the gas-invaded area reduces the fracture opening. The fracture permeability decreases. At this stage, the coal permeability is controlled primarily by the internal structure. As the gas-invaded area expands from the vicinity of the fracture wall to the outside of the matrix, the fracture opening may rebound depending on the external boundary conditions. When the gas spreads all over the matrix, the final equilibrium state between the matrix and the fracture is achieved. After the final equilibrium state is reached, the whole coal volume swells, so does the fracture opening. Therefore, the coal permeability reaches a magnitude higher than the initial one at the final equilibrium state. This conceptual understanding of permeability four-stage evolutions (initial increase due to fracture inflation, decrease due to local swelling, rebound due to global swelling, and stabilization due to uniform swelling) is correlated to the matrix strain difference quite well.

3. A strain-rate based permeability model

In this section, we formulated the correlation between fracture permeability and matrix strain difference through a strain-rate based model. Based on theory of linear poroelasticity, fracture deformation is determined by the effective stress in the fracture system. The simulation results of explicit geometry indicate that effect of non-uniform
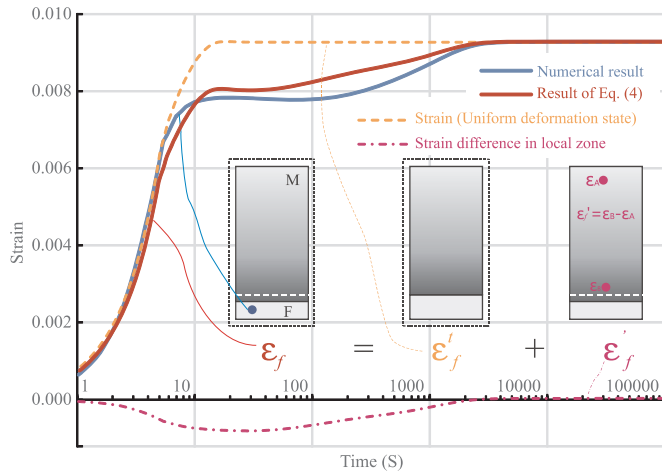
Fig. 7. Illustration of the fracture strain definition.

deformation on fracture permeability is dependent on the strain difference adjacent to fracture. Therefore, the effective stress is also dependent on the interactions between fracture and matrixes. In this study, we decompose the fracture strain into two components: One is the strain induced by the uniform fracture deformation. The strain changes with effective stress. This is the traditional method.[5] The other is the strain induced by the strain variation within the matrix. In this study, we define the non-uniform strain contribution as the local strain. This strain is due to the localization at the initial state and will evolve into a uniform state when the final equilibrium state is reached. The total fracture strain is defined as

$$\varepsilon_f = \varepsilon_f^t + \varepsilon_f' \tag{4}$$

where ε_f is the fracture strain, ε_f^t is the uniform strain component, ε_f' is the non-uniform strain component. The assumption here is that the non-uniform strain component can be considered as the strain difference in matrix.

Fig. 7 illustrates the definition of the fracture strain as defined by Eq. (4). According to Eq. (4), the red solid curve is the summation of the

uniform strain (orange dash curve) and the local matrix strain (purple dash curve). The uniform strain is the model results of single porous medium ($k_f/k_m = 1$). For the comparison, the blue line is the model result $k_f/k_m = 100$, which denotes the fracture strain. Comparing blue line and the red line shows that the result of Eq. (4) is consistent with the numerical result in Section 2.2. Fracture strain increases with the decrease of effective stress in the beginning. Meanwhile, the strain in matrix increases because of the decrease of gas pressure. Subsequently, fracture subjected the compressional activity from swelling matrix. When the gas pressure is uniform in the whole system, the strain curve keeps steadily.

As discussed above, there exists an influence of non-uniform deformation of the matrix on fracture aperture when the difference between fracture and matrix permeability is large. However, dual-porosity implementations neglect spatial variation within local matrix regions. Models of this type are well-suited for some purposes but are limited in their ability to represent this effect, as spatial variation within the matrix is not modeled.

The local strain in the matrix is generated due to the spatial distribution of the non-uniform deformation. However, the physical parameters in matrix block are incorporated into a single point for conventional dual porosity/permeability model. This approach lost the information of spatial variation in the matrix. Since the physical positions of matrix and fracture are overlapping to each other, the interaction between these two systems is formulated within the representative point. In this framework, the connecting blocks in space distribution can also be considered as itself because they have the same physical parameters. The deformation in the representative block is uniform in spatial distribution but is variable with time. If two blocks are overlapped at one point in space, the compression between two adjacent blocks can be considered as the ratio of deformation change from itself as illustrated by Fig. 8. In other words, the impact from matrix can be considered as the ratio of matrix deformation change. Fracture deformation is affected by this impact, which shares the same spatial position. The transform of space to time means that local strain effect in space distribution can be replaced by the change ratio. Similarly, based on the assumption that the local strain is generated by the gas pressure change induced strain difference between fracture and matrix, it is reasonable to reformulate the local strain as:
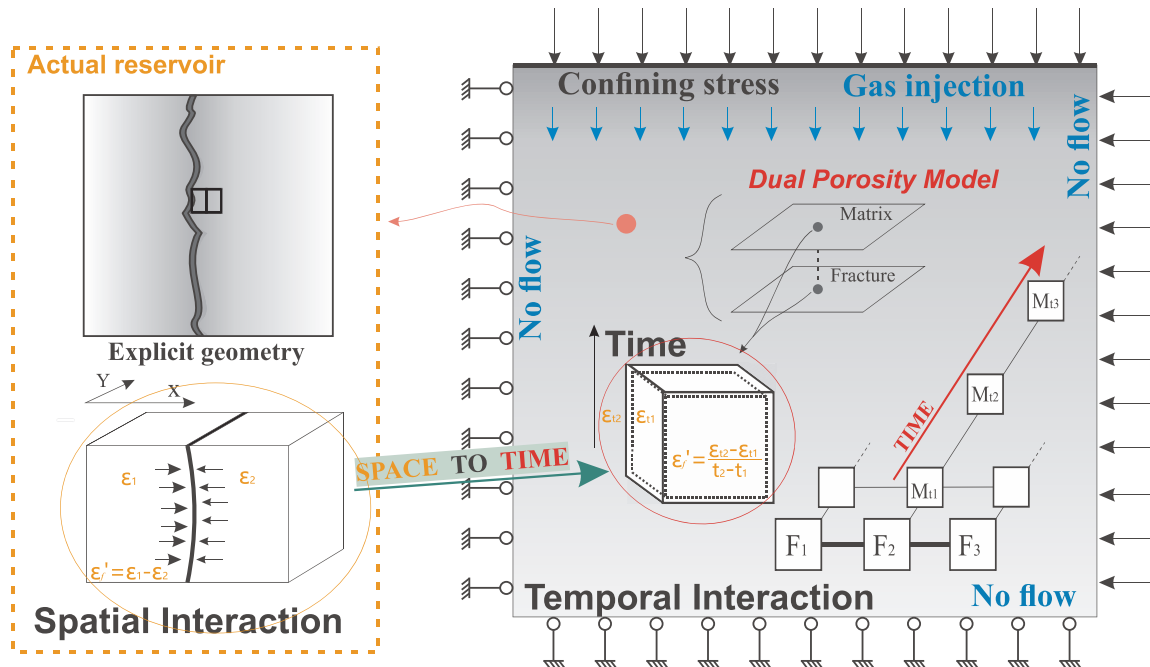

Fig. 8. Schematic of the numerical simulation model.

$$\varepsilon'_f = \gamma \frac{\Delta \varepsilon_m}{t_2 - t_1} = \gamma \frac{\partial}{\partial t}\left(-\frac{\Delta p_m}{K_m} + \Delta \varepsilon_s\right) \varepsilon_s = \varepsilon_L \frac{P_m}{p_m + L_b} \qquad (5)$$

where ε'_f is the time-dependent local strain in fracture, ε_m is the matrix strain, $\Delta\varepsilon_s$ is the gas sorption-induced volumetric strain increment of matrix,?? is a characteristic time factor, it represents the time eventually scaling the non-uniform strain component at the macroscopic level. Based on Eq. (4), the total strain in fracture is:

$$\varepsilon_f = \varepsilon^t_f + \gamma \frac{\partial}{\partial t}\left(-\frac{\Delta p_m}{K_m} + \Delta \varepsilon_s\right) \qquad (6)$$

Based on the fundamental poroelasticity, the fracture permeability can be defined as a function of effective strain (Zhang et al.[5]; Liu et al.[10]):

$$\frac{k_f}{k_{f0}} = \left(\frac{\phi_f}{\phi_{f0}}\right)^3 = \left(1 + \frac{\alpha}{\phi_{f0}}\left(\Delta\varepsilon_f - \frac{p_f}{K_s}\right)\right)^3 \qquad (7)$$

where ϕ_{f0} and k_{f0} are the initial porosity and permeability of fracture, α is the Biot coefficient, K_s is the bulk modulus of the matrix. Substituting Eq. (6) into Eq. (7) yields:

$$\frac{k_f}{k_{f0}} = \left(\frac{\phi_f}{\phi_{f0}}\right)^3 = \left(1 + \frac{\alpha}{\phi_{f0}}\left(\Delta\left(\varepsilon^t_f + \gamma\frac{\partial}{\partial t}\left(-\frac{\Delta p_m}{K_m} + \Delta\varepsilon_s\right)\right) - \frac{p_f}{K_s}\right)\right)^3 \qquad (8)$$

This new permeability model fully considers the effect of local strain from the matrix and effective stress. In the following sections, this new model is applied to a series of cases to generate typical response curves.

4. Model verifications and sensitivity studies

In this section, we verified our strain-rate based model through comparing the model results with the experimental ones conducted by Liu et al.[22]. In this experiment, the permeability evolution as a function of the adsorption equilibrium time was measured under the constant stress boundary. A case of numerical model was built according to the experimental condition as shown in Fig. 8. The model size of 50×100 mm is same as the experimental sample. Constant confining stresses were applied on boundaries. CO_2 was injected from the top boundary and no flow conditions are applied on all other boundaries. A dual permeability model was used in this simulation. The coal sample can be assumed as a linearly elastic, homogeneous, isotropic material. In addition, the gas flows in matrix and fracture are governed by Darcy's law. The governing equations for matrix and fracture are defined as Eqs. (1) through (3). All the equations are implemented and solved numerically using COMSOL Multiphysics simulation software. The fracture permeability is defined as Eq. (8). The other parameters are constant. The input parameters for the model are listed in Table 2.

The comparison between experimental data and model results is plotted in Fig. 9. The experiment was conducted for 168 h to reach an
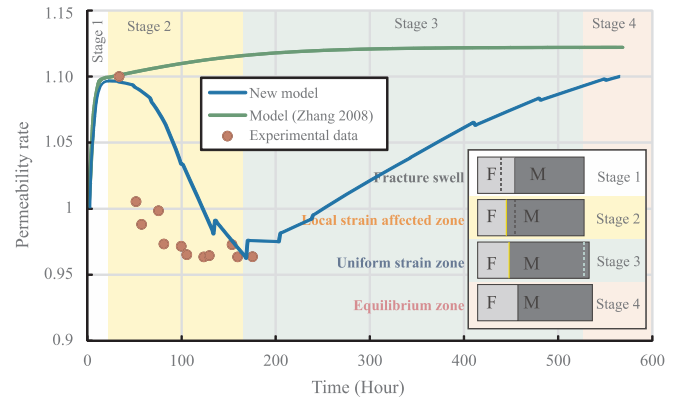
Table 2
Property parameters of simulation model.

Parameters	Value
Young's modulus of bulk	8 GPa
Young's modulus of matrix	10 GPa
Possion's ratio	0.27
Biot coefficient	1
Initial porosity of matrix	0.02
Initial porosity of fracture	0.02
Initial permeability of matrix	1×10^{-19} m^2
Initial permeability of fracture	3×10^{-16} m^2
Confining pressure	2.068 MPa
Injection pressure	0.689 MPa
Langmuir volume constant	28.6308 m^3/t
Langmuir pressure	1.6136 MPa
Time factor	1×10^6 s

Fig. 9. Comparison between the model results and experimental data.

equilibrium state. The first permeability data point of the coal sample was obtained approximately 24 h after the injection. With the progress of gas adsorption in matrix, experimental data continually decreases for 80 h. Then, in the later 70 h, the permeability keeps steady until the end of the experiment. As reviewed in the introduction, conventional permeability models consider permeability change as a result of mechanical strain and coal swelling/shrinkage.[5,28,29] The curve of the model result from[5] was plotted in green. Coal permeability increases with the adsorption equilibrium time. It is obviously that this model based on equilibrium state assumption fails to predict the permeability change. According to Eq. (8), the model curve follows a similar pattern to that of the experimental results. The evolution of permeability based on our new model can be divided into four stages: (1) Stage 1 Permeability Increase. Permeability increases rapidly right after the injection. The trend of our new model result coincides with the results of Zhang's model.[5] This coincidence indicates that the effect of effective stress in the fracture system is dominant; (2) Stage 2 Permeability Decrease. As the gas diffuses from fractures to matrix blocks, the gas pressure in matrix increases. This pressure increase leads to the swell of the matrix near to the fracture. This localization of swelling reduces the fracture aperture. This reduction in aperture decreases the permeability. In this stage, the effect of local strain in matrix is dominant; (3) Stage 3 Permeability Recovery. As the gas propagates from the vicinity of the fracture wall to the exterior region, the matrix strain becomes more uniform. In this stage, the effect of local strain in the matrix vanishes; The stage could last months or years before a final equilibrium state is reached; (4) Stage 4 Permeability Stablization. When a final equilibrium state is reached, the effect of local strain completely vanishes and the permeability remain unchanged. Although the experimental data show two stages only, our model results capture the whole evolution from Stage 1 to Stage 4.

When the initial fracture permeability remains unchanged, the effects of matrix-to-fracture permeability ratios on the evolution of permeability are shown in Fig. 10. As the permeability ratio increases (the matrix becomes more permeable), the permeability valley becomes shallower. This is consistent with the conclusion of Fig. 6. It proves that the permeability ratio of matrix and fracture is main cause for local strain effect.

5. Impact of permeability evolution on gas production

Precise prediction of permeability in coal seam is important to determine CBM productivity.[30] To evaluate the impact of permeability evolution on gas production, a simulation case of up-scaled geometry is built based on dual-porosity model. Coal is assumed as a homogeneous, a homogeneous, isotropic, and elastic medium.[30] The gas mass in the matrix exists in both adsorption and free phase. The gas mass balance equation in the matrix can be expressed as[31]:
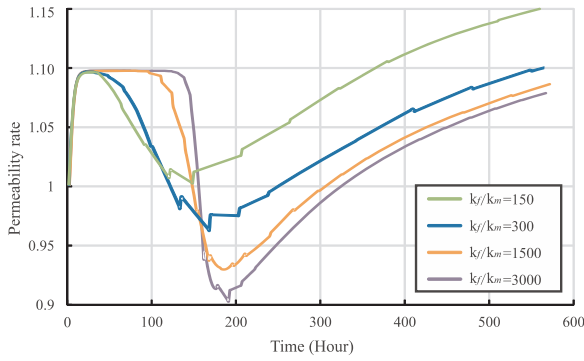
Fig. 10. Illustration the effect of matrix-to-fracture permeability ratios on the evolution of permeability.

$$\frac{\partial}{\partial t}\left(\phi_m \rho_m + (1-\phi_m)\rho_s \rho_a \frac{L_a P_m}{P_m + L_b}\right) + \nabla\left(-\rho_m \frac{k_m}{u}\nabla P_m\right) = -Q_{mf} \tag{9}$$

where ϕ_m and k_m are the porosity and permeability of matrix, ρ_m is the gas density, ρ_s is shale density, ρ_a is gas density at atmospheric pressure in kerogen system, L_a represents the Langmuir volume constant, L_b represents the Langmuir pressure, P_m is the pore pressure in matrix, u is gas viscosity. The mass transfer from matrix to fracture can be considered as diffusion process. The mass exchange depends on the concentration difference between two continua at the interface that can be simplified as:

$$Q_{mf} = a_{mf} D_{mf}(\rho_m - \rho_f) \tag{10}$$

where a_{mf} is a shape factor, D_{mf} is diffusion coefficient.

Because the most efficient transport mechanism is pressure-driven volume flow, Darcy flow is dominant in fracture networks. The gas mass balance equation in the fracture is given as:

$$\frac{\partial}{\partial t}(\phi_f \rho_f) - \rho_f \frac{k_f}{u}\nabla P_f = Q_{mf} \tag{11}$$

where ϕ_f is the porosity of natural fracture, k_f is the permeability of fracture, P_f is the gas pressure in the fracture, ρ_f is the gas density in fracture system.

The geometry model of coal reservoir has length of $1000 \times 1000 \times 5\,\text{m}$. The drainage well with $200\,\text{mm}$ in diameter is located in the central. Detailed reservoir information and parameters used in simulations are all listed in Table 3.

The permeability of coal reservoirs changes significantly during gas production as shown in Fig. 11. For comparison purposes, four cases were conducted with different fracture permeability model. The fracture permeability is constant in the case of one. The case of two is based on Eq. (7). The fracture permeability declines when the gas pressure is drawn down. So the permeability ratio in the fracture drops from one to

Table 3
Values of variables used for the simulation.

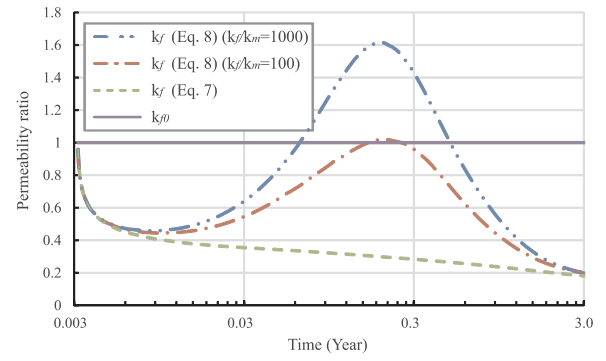| Parameter	Value
Model dimension (length × width × height)	$1000 \times 1000 \times 5\,\text{m}$
Initial reservoir pressure	4 MPa
Wellbore pressure	1 MPa
Langmuir volume constant, L_a	$28.6308\,\text{m}^3/\text{t}$
Langmuir pressure, L_b	1.6136 MPa
Coal density, ρ_s	$1580\,\text{kg/m}^3$
Gas viscosity, u	$1.84 \times 10^{-5}\,\text{Pa s}$
Shape factor, a_{mf}	1
Diffusion coefficient, D_{mf}	$1 \times 10^{-8}\,\text{m}^2/\text{s}$
Initial porosity of matrix ϕ_{m0}	2%
Initial fracture porosity, ϕ_{f0}	2%
Initial permeability of matrix, k_{m0}	$1 \times 10^{-19}\,\text{m}^2$
Initial fracture permeability, k_{f0}	$1 \times 10^{-16}\,\text{m}^2$

Fig. 11. Change of fracture permeability during gas production.

0.2 for three years of gas production. This model fails to account for the local effect of the matrix. The results of the other two cases show that the permeability ratio is non- monotonically decreasing. It n initially decreasing but then increasing as the reservoir pressure is drawn down. The rebound stage responses to the local strain induced by matrix shrinkage. When the matrix deformation reaches uniform, the impact on fracture permeability vanishes. Then the permeability ratio continues the downward trend. It is obvious that the rebound is higher with a greater difference between matrix and fracture permeability. When the gas reaches equilibrium pressure in the matrix after three years, the permeability ratios are close for the case of two, three and four. Fig. 12 shows the cumulative production of gas for four cases. As can be seen, the gas production is highest when fracture permeability keeps constant. The simulation result with Eq. (7) is lowest due to the rapid decline of permeability after gas production. Since the fracture permeability rebounds, the gas production increases when the local effect is included. It indicates that previous permeability models underestimated the gas production.

6. Conclusions

Because coal matrix and fractures have dramatically different mechanical properties, the partial contributions of matrix swelling/shrinkage affects the evolution of fracture aperture. This interaction can have a significant effect on permeability changes under certain conditions. In this study, we developed a strain rate-based permeability model to quantify the effects of the gas diffusion-induced non-uniform matrix deformation on the evolution of coal permeability. Based on model results, the following conclusions can be drawn.

Under the condition of constant confining stresses, coal permeability normally experiences four distinctive stages for the case of gas injection: permeability increases due to the injection pressure, permeability decrease due to the localization of matrix strain change; permeability recovery due to the globalization of matrix strain change; permeability stabilization due to the establishment of final equilibrium state.
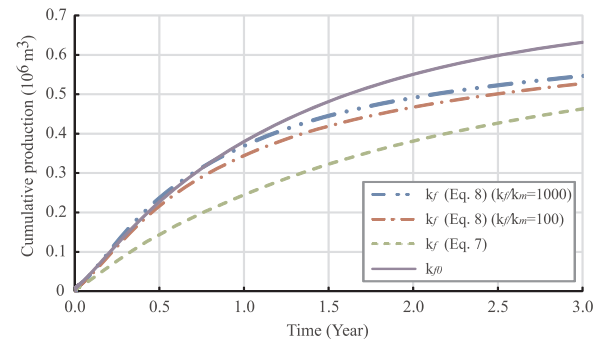

Fig. 12. Cumulative production for four cases.

The four-stage evolutions of coal permeability are regulated by the initial fracture-to-matrix permeability ratios. When the ratio is small, two intermediate stages may disappear and the response of coal permeability to gas injection is linear. When the ratio is large, all four stages may be significant and the response of coal permeability is a valley shape.

The fracture permeability declines with decrease of gas pressure when gas production initially. But then it rebounds due to the local strain induced by matrix shrinkage. The rebound is higher with a greater difference between matrix and fracture permeability. When the gas reaches equilibrium pressure in the matrix after years of production, the permeability continues the downward trend.

Acknowledgments

References

1. Mitra A, Harpalani S, Liu S. Laboratory measurement and modeling of coal permeability with continued methane production: Part 1 – laboratory results. *Fuel.* 2012;94:110–116.
2. Gray I. Reservoir engineering in coal seams: Part 1 – the physical process of gas 587 storage and movement in coal seams. *SPE Reserv Eng.* 1987;2:28–34.
3. Palmer I, Mansoori J. How permeability depends on stress and pore pressure in coalbeds: a new model. *SPE Reserv Eval Eng.* 1996;1:539–544.
4. Shi JQ, Durucan S. Drawdown induced changes in permeability of coalbeds: a new interpretation of the reservoir response to primary recovery. *Trans Porous Media.* 2004;56:1–16.
5. Zhang HB, Liu JS, Elsworth D. How sorption-induced matrix deformation affects gas flow in coal seams: a new FE model. *Int J Rock Mech Min Sci.* 2008;45:1226–1236.
6. Cui X, Bustin RM, Chikatamarla L. Adsorption-induced strain and permeability increase with depletion for CBM reservoirs. In: *SPE Annual Technical Conference and Exhibition.* Denver, USA; 2008.
7. Jin Y, Zhu YB, Li X, et al. Scaling invariant effects on the permeability of fractal porous media. *Trans Porous Media.* 2015;109(2):433–453.
8. Niu QH, Cao LW, Sang SX, et al. Anisotropic adsorption swelling and permeability characteristics with injecting CO_2 in coal. *Energy Fuels.* 2018;32(2):1979–1991.
9. Zhu WC, Liu LY, Liu JS, et al. Impact of gas adsorption-induced coal damage on the evolution of coal permeability. *Int J Rock Mech Min Sci.* 2018;101:89–97.
10. Liu JS, Chen ZW, Elsworth D, et al. Interactions of multiple processes during CBM extraction: a critical review. *Int J Coal Geol.* 2011;87(3):175–189.
11. Zhang XG, Ranjith PG, Perera MSA, et al. Gas transportation and enhanced coalbed methane recovery processes in deep coal seams: a review. *Energy Fuels.* 2016;30(11):8832–8849.
12. Zimmerman RW. Pore volume and porosity changes under uniaxial strain conditions. *Transp Porous Media.* 2017;119(2):481–498.
13. Liu HH, Rutqvist J. A new coal-permeability model: internal swelling stress and fracture-matrix interaction. *Trans Porous Media.* 2010;82:157–171.
14. Wang CG, Feng JL, Liu JS, et al. Direct observation of coal–gas interactions under thermal and mechanical loadings. *Int J Coal Geol.* 2014;131:274–287.
15. Peng Y, Liu JS, Wei MY, et al. Why coal permeability changes under free swellings: new insights. *Int J Coal Geol.* 2014;133:35–46.
16. Qu HY, Liu JS, Pan ZJ, et al. Impact of matrix swelling area propagation on the evolution of coal permeability under coupled multiple processes. *J Nat Gas Sci Eng.* 2014;18:451–466.
17. Shi R, Liu JS, Wei MY, et al. Mechanistic analysis of coal permeability evolution data under stress-controlled conditions. *Int J Rock Mech Min Sci.* 2018;110:36–47.
18. Liu JS, Wang JG, Chen ZW, et al. Impact of transition from local swelling to macro swelling on the evolution of coal permeability. *Int J Coal Geol.* 2011;88:31–40.
19. Siriwardane H, Halkasmaa I, Mclendon R, et al. Influence of carbon dioxide on coal permeability determined by pressure transient methods. *Int J Coal Geol.* 2009;77:109–118.
20. Chen ZW, Pan ZJ, Liu JS, et al. Effect of the effective stress coefficient and sorption-induced strain on the evolution of coal permeability: experimental observations. *Int J Greenh Gas Cont.* 2011;5:1284–1293.
21. Perera MSA, Ranjith PG, Choi SK, et al. Investigation of temperature effect on permeability of naturally fractured black coal for carbon dioxide movement: an experimental and numerical study. *Fuel.* 2012;94:596–605.
22. Liu QQ, Cheng YP, Ren T. Experimental observations of matrix swelling area propagation on permeability evolution using natural and reconstituted samples. *J Nat Gas Sci Eng.* 2016;34:680–688.
23. Ranathunga AS, Perera MSA, Ranjith PG, et al. Super-critical CO_2 saturation-induced mechanical property alterations in low rank coal: an experimental study. *J Supercrit Fluids.* 2016;109:134–140.
24. Wang Y, Liu SM. Estimation of pressure-dependent diffusive permeability of coal using methane diffusion coefficient: laboratory measurements and modeling. *Energy Fuels.* 2016;30(11):8968–8976.
25. Nie BS, Fan PH, Li XC. Quantitative investigation of anisotropic characteristics of methane-induced strain in coal based on coal particle tracking method with X-ray computer tomography. *Fuel.* 2018;214:272–284.
26. Zhang SW, Liu JS, Wei MY, et al. Coal permeability maps under the influence of multiple coupled processes. *Int J Coal Geol.* 2018;187:71–82.
27. Wu Y, Liu JS, Elsworth D, et al. Dual poroelastic response of a coal seam to CO_2 injection. *Int J Greenh Gas Cont.* 2010;4:668–678.
28. Seidle JP, Jeansonne MW, Erickson DJ. Application of matchstick geometry to stress-dependent permeability in coals. In: *SPE Rocky Mountain Regional Meeting.* Casper, Wyoming: U.S.; 1992.
29. Harpalani S, Chen G. Influence of gas production induced volumetric strain on permeability of coal. *Geotech Geol Eng.* 1997;15:303–325.
30. Wu YT, Pan ZJ, Zhang DY, et al. Evaluation of gas production from multiple coal seams: a simulation study and economics. *Int J Min Sci Technol.* 2018;28:3.
31. Wei MY, Liu JS, Elsworth D, et al. Triple-porosity modelling for the simulation of multiscale flow mechanisms in shale reservoirs. *Geofluids.* 2018 [ID 6948726].